Journal of Power Sources 183 (2008) 498–505

Contents lists available at ScienceDirect

Journal of Power Sources

journal homepage: www.elsevier.com/locate/jpowsour

Electrical properties of Mg-doped $Gd_{0.1}Ce_{0.9}O_{1.95}$ under different sintering conditions

Bin Li, Xi Wei, Wei Pan*,[1]

State Key Lab. of New Ceramics and Fine Processing, Department of Materials Science and Engineering, Tsinghua University, Beijing 100084, People's Republic of China

ARTICLE INFO

Article history:
Received 27 April 2008
Received in revised form 9 May 2008
Accepted 20 May 2008
Available online 27 May 2008

Keywords:
Solid oxide fuel cells
Ceria
Grain boundary conductivity
Sintering conditions

ABSTRACT

$Ce_{0.9}Gd_{0.1}O_{1.95}$ with various Mg doping contents was synthesized by citric acid-nitrate low temperature combustion process and sintered under different conditions. The crystal structures, microstructures and electrical properties were characterized by X-ray diffraction (XRD), field-emission scanning electron microscopy (FESEM) and ac impedance spectroscopy. Low solubility of Mg^{2+} in $Ce_{0.9}Gd_{0.1}O_{1.95}$ lattice was evidenced by XRD and FESEM micrographs. The samples sintered at 1300 °C exhibited the higher total conductivity than those sintered at 1100 and 1500 °C, with the maximum value of 1.48×10^{-2} S cm^{-1} (measured at 600 °C) at the Mg doping content of 6 mol%, corresponding to the minimum total activation energy (E_{tol}) of 0.84 eV (150–400 °C). The effect of Mg doping on the electrical conductivity was significant particularly at higher sintering temperatures. At the sintering temperature of 1500 °C, the addition of Mg (10 mol%) enhanced the grain boundary conductivity by over 10^2 times comparing with that of undoped $Ce_{0.9}Gd_{0.1}O_{1.95}$, which may be explained by the optimization of space charge layer due to the segregation of Mg^{2+} to the grain boundaries.

1. Introduction

Solid oxide electrolytes based on doped ceria, $Ce_{1-x}M_xO_{2-\delta}$ (M: rare-earth or alkaline-earth cations), are of considerable interest for potential use in solid oxide fuel cells (SOFCs), oxygen sensors, oxygen pumps, and so on. Gadolinia (GDC) or samaria-doped ceria (SDC) were confirmed to be attractive electrolytes [1–3]. They exhibit higher ionic conductivity possibly because they minimize the changes in lattice parameters, as reported by Kim [4]. In addition, some atomistic simulations based on the binding energy between trivalent cations and oxygen vacancies, and the corresponding lattice relaxation energy suggest the optimum radius for the trivalent cations should be close to that of Gd^{3+} [5].

Recently, lowering the operating temperature has become a tendency to research on the solid oxide electrolytes by reason of the potential use of cheaper construction materials and more reliable seals, as well as long lifetimes of the devices. However, lower temperature retards the oxygen diffusion in the grain interior (the bulk) of the electrolytes, especially across the grain boundary. This is ascribed to the higher activation energy of the grain boundary conductivity than that in the grain [6,7]. As described by Guo and Waser [8], generally, the total grain boundary resistance (R_{gb}) consists of two contributions: the resistance $R_{gb}1$ resulting from the segregation of SiO_2 or other impurities at the grain boundary, which decreases the contact areas of the conductive grains; the resistance $R_{gb}2$ resulting from the depletion of oxygen vacancies near the grain boundary due to the formation of the space charge layer. For the sample (SiO_2 wt.% < 50 ppm), $R_{gb}1$ is thought to be negligible, and the grain boundary resistance is believed to be proposed only by space charge depletion layer [8]. In order to reduce the grain boundary resistance and the activation energy, selecting an appropriate additive has become a hot spot. Up to now, very few additives have been found to take effects on the reduction of both $R_{gb}1$ and $R_{gb}2$ except Fe_2O_3. The alkaline earth metal oxides, such as MgO, CaO and SrO, have only been found to play a role in reducing $R_{gb}1$. As investigated by Cho et al. [9–11], MgO and SrO were used as SiO_2 scavengers by the reaction with SiO_2 and gathering at triangle regions of grain boundaries, and the addition of CaO induced the configuration change in the grain-boundary segregation. Fe_2O_3 [12,13] was also confirmed to be the effective additive to scavenge the siliceous phase. However, except Fe_2O_3, some other transition metal oxides (TMOs), such as Co_2O_3 and Mn_2O_3, have been found to only take effect on reducing $R_{gb}2$ by altering the distribution of oxygen vacancies near the grain boundary [12–15]. This kind of additives must satisfy a precondition, that is, very low solubility in

* Corresponding author. Tel.: +86 10 62782283; fax: +86 10 62771160.
E-mail addresses: bli05@mails.tsinghua.edu.cn (B. Li), panw@mail.tsinghua.edu.cn (W. Pan).
[1] Tel.: +86 10 62772858; fax: +86 10 62771160.

0378-7753/$ – see front matter © 2008 Elsevier B.V. All rights reserved.
doi:10.1016/j.jpowsour.2008.05.050

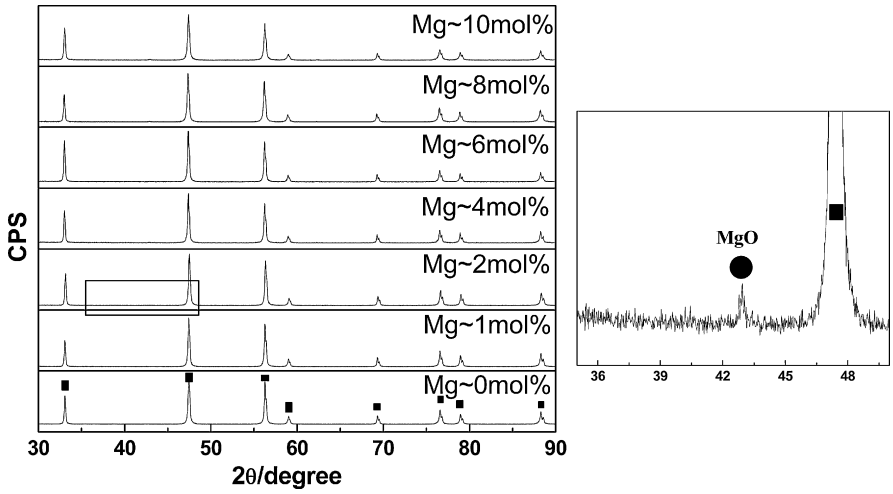

Fig. 1. XRD patterns of Mg-doped $Ce_{0.9}Gd_{0.1}O_{1.95}$ sintered at 1300 °C for 4 h (■, $Ce_{0.9}Gd_{0.1}O_{1.95}$; ●, MgO).

matrix lattice. However, as a result of some TMOs with electric conductance, a very small amount of TMOs were needed in case TMOs may be formed in the grain boundary serving as a fast conduction path for electrons [14]. It is known MgO is an insulating material and cannot lead to the electric conduction. Moreover, besides the scavenging effect [9], the addition of MgO may reduce $R_{gb}2$ for the ceria-based electrolytes.

It is noteworthy that sintering condition is a critical factor to influence the electrical property, particularly the grain boundaries', which can bring about some difficulties on obtaining high-performance electrolytes. For example, Li et al. [16] found that $Ce_{0.8}Sm_{0.2}O_{1.9}$ sintered at 1400 °C showed considerably lower conductivity than that sintered at 1200–1300 °C, and they suggested the lower conductivity should be attributed to the well developed space charge regions at the grain boundary at higher sintering temperatures. Both Sha et al. [7] and Qu et al. [17] have also found the same phenomenon.

In the present work, $Ce_{0.9}Gd_{0.1}O_{1.95}$ was chosen to be the base electrolyte because of its high grain conductivity and better stability at low oxygen partial pressure [18]. The samples with different amount of MgO addition were prepared by citric acid-nitrate low temperature combustion process. The effects of MgO on electrical properties were investigated under different sintering conditions.

2. Experimental

$Ce_{0.9}Gd_{0.1}O_{1.95}$ with and without MgO doping were synthesized by citric acid-nitrate low temperature combustion process [19]. Analytical reagents $Ce(NO_3)_3{\cdot}6H_2O$ (≥99.9 wt.%, Yutai Qingda, China), $Gd(NO_3)_3{\cdot}6H_2O$ (≥99.9 wt.%, Yutai Qingda, China), $Mg(NO_3)_2{\cdot}6H_2O$ (≥99.0 wt.%, Modern Eastern, China), and $C_6H_8O_7{\cdot}H_2O$ (≥99.0 wt.%, Modern Eastern, China) were used as starting materials. The molar ratio of the metal ions to citric acid was 1:1.2. Stoichiometric amounts of $Ce(NO_3)_3{\cdot}6H_2O$, $Gd(NO_3)_3{\cdot}6H_2O$ and $Mg(NO_3)_2{\cdot}6H_2O$ were dissolved in proper deionized water to form transparent solution. The total concentration of metal ions was controlled to be about 0.1 mol/l. Then citric acid was added into the solution with stirring for about 1 h. The transparent solution was heated at 95 °C in a water bath until the yellow gel was yielded, and then dried in a constant temperature drying oven at 80 °C for 12 h. The dried gel was heated in the air on the electric oven and self-ignited until the yellow powders without black carbons were generated. Mg-doped $Ce_{0.9}Gd_{0.1}O_{1.95}$, containing 0, 1, 2, 4, 6, 8 and 10 mol% MgO, were synthesized by that method. SiO_2 content of the powders, which was characterized by inductively coupled plasma mass spectroscopy (ICP, X Series), was about 42 ppm. The powders were sieved to 100 meshes, uni-axially dry-pressed into pellets (φ 10 mm) under 200 MPa, and then sintered at different sintering temperatures (1100, 1300 and 1500 °C) for 4 h. All the specimens were sintered in air and heated by the rate of 240 °C h^{-1}, and then furnace-cooled after sintering. Densities of the sintered pellets were determined by Archimedean method.

Phase identification and analysis were conducted by X-ray diffraction (XRD). Two kinds of XRD scans were performed using an X-ray diffractometer (Rigaku, D/max-RB, Japan) with nickel-filtered Cu Kα radiation. Continuous scans (6° min^{-1}) were used for qualitative phase identification, while slow step scans at a rate of 0.02°/2 s were conducted to determine the shifts of the X-ray spectrum and hence the lattice parameters. Lattice parameters of the specimens were calculated from slow step scan XRD data, using the least-squares method. The sintered pellets were polished, thermally etched, and carbon coated for microstructural analysis using field-emission scanning electron microscopy (FESEM, JSM-6301F) equipped with an energy-dispersive X-ray spectrometer (EDX) analyzer. The average grain sizes were obtained from FESEM micrographs of the etched samples by using the linear intercept technique described by Mendelson [20]. The grain and grain

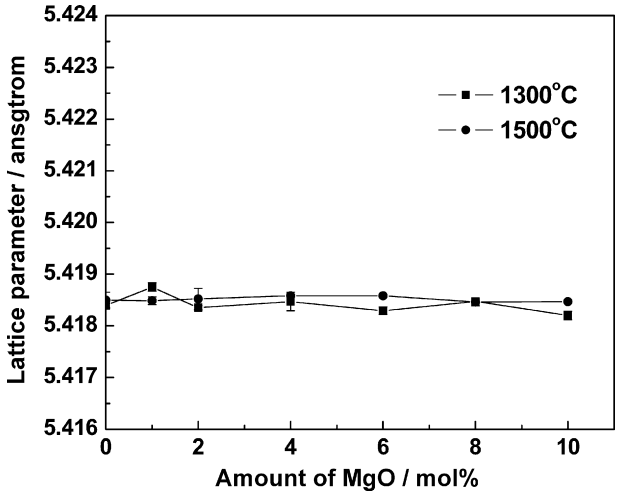

Fig. 2. Lattice parameters of the samples sintered at different temperatures vs. MgO concentration.

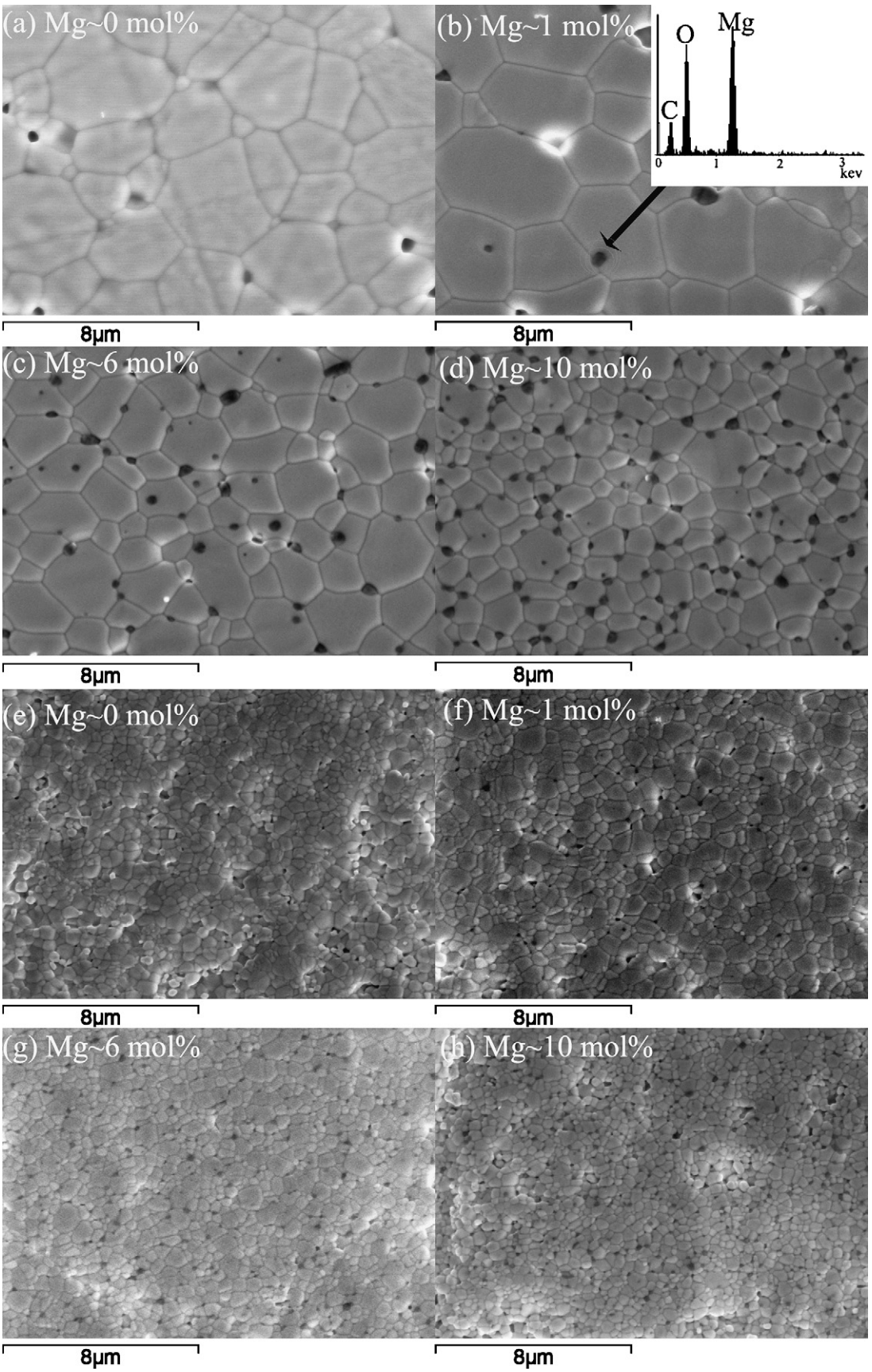

Fig. 3. FESEM micrographs of Mg-doped $Ce_{0.9}Gd_{0.1}O_{1.95}$ sintered at 1500 °C (a–d) and 1300 °C (e–h) for 4 h. The inset of Fig. 3(b) is the EDX result of dark phase.

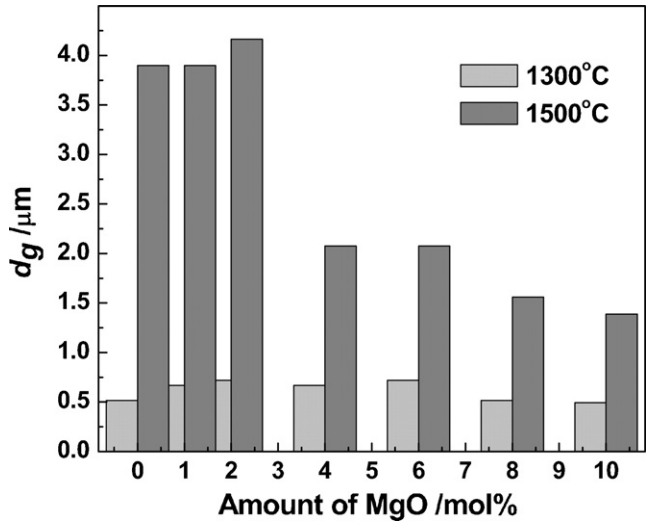

Fig. 4. Average grain size (d_g) of the $Ce_{0.9}Gd_{0.1}O_{1.95}$ specimens with various MgO doping concentrations. All the specimens were sintered at 1300 and 1500 °C for 4 h.

boundary conductivities in air were determined by ac impedance spectroscopy (IM6, German). Silver electrodes were coated on both surfaces of the sintered pellets and heated at 550 °C for 30 min. Impedance measurement was performed on heating from 150 to 600 °C in a frequency range from 0.1 Hz to 8 MHz with an increment of 50 °C, and followed by analyzing these results using Z-View software.

3. Results and discussion

Fig. 1 shows the XRD patterns of Mg-doped $Ce_{0.9}Gd_{0.1}O_{1.95}$ with 0, 1, 2, 4, 6, 8 and 10 mol% MgO sintered at 1300 °C for 4 h from a continuous scan. The undoped and 1 mol% Mg-doped $Ce_{0.9}Gd_{0.1}O_{1.95}$ specimens show a pure cubic structure. A small MgO peak appears when the amount of Mg is up to 2 mol%. With the increasing MgO additions, the intensity of peaks corresponding to MgO phase is increased and no additional extraneous peaks are observed indicating that no distinct chemical interactions with the matrix have taken place. Also, no noticeable peak shift is observed which indicates the solubility of MgO in $Ce_{0.9}Gd_{0.1}O_{1.95}$ is minimal. Fig. 2 shows the lattice parameters of the samples sintered at different temperatures versus MgO concentration. It can be seen that the lattice parameter keeps the value of 5.418 Å, independent of the doping content and sintering temperatures. Because of much smaller radius of Mg^{2+} (0.89 Å) than that of Ce^{4+} (0.97 Å) [21], substituting Mg^{2+} for Ce^{4+} can certainly induce the variation of

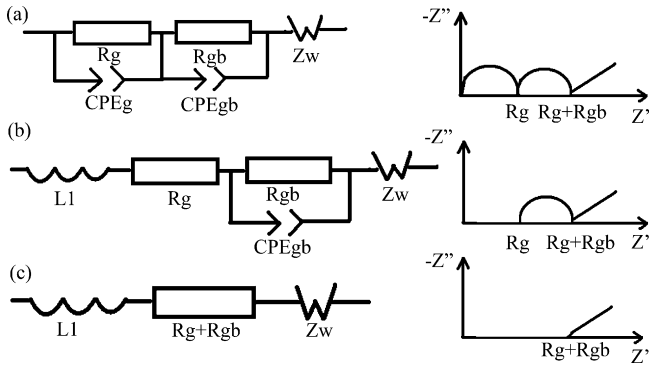

Fig. 5. Different schematic equivalent circuits and corresponding ac impedance responses, where L_1, R_g, R_{gb}, CPE_g, CPE_{gb} and Z_w represent inductance of the experiment setup, grain resistance, grain boundary resistance, constant phase element of the grain, constant phase element of the grain boundary and Warburg impedance, respectively.

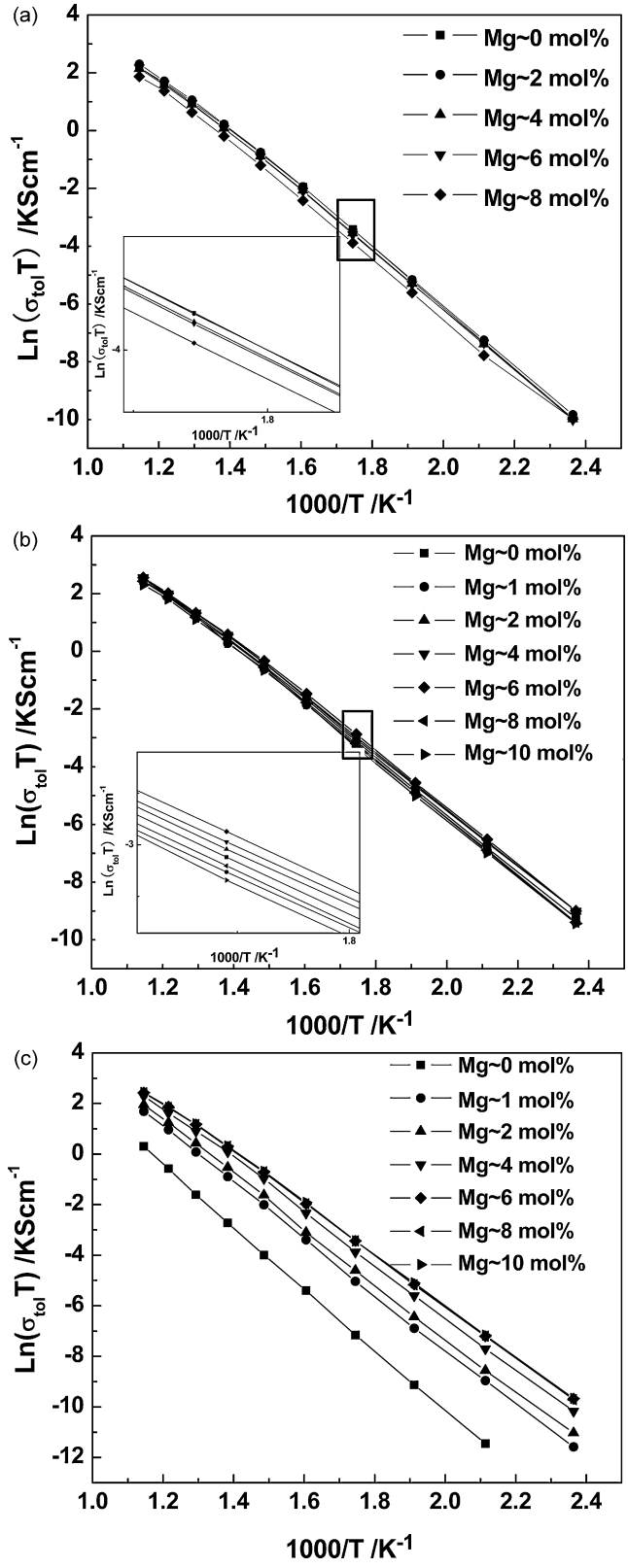

Fig. 6. The total conductivity (σ_{tol}) of the samples with various Mg concentrations: (a) sintered at 1100 °C; (b) sintered at 1300 °C; (c) sintered at 1500 °C.

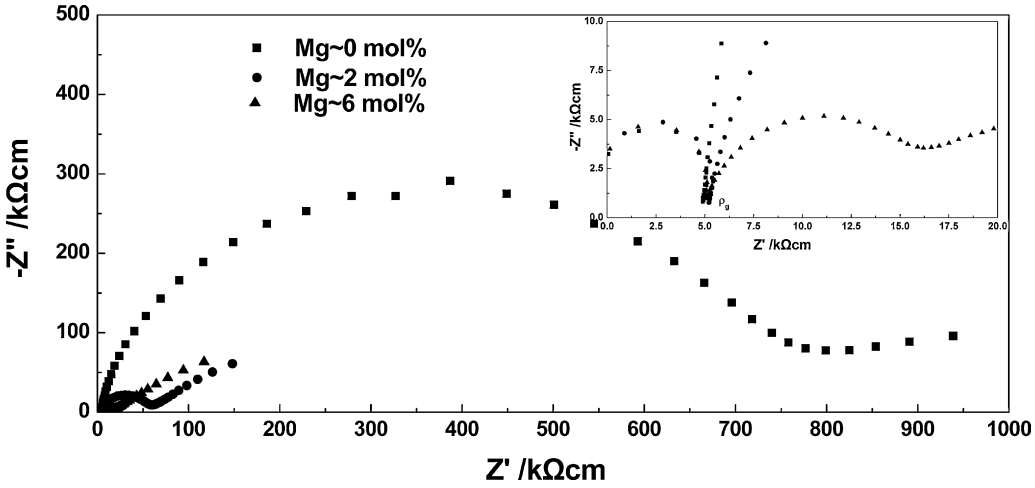

Fig. 7. The ac impedance spectra of the samples (sintered at 1500 °C for 4 h) with various Mg concentrations measured at 300 °C in air.

lattice parameter. Hence, the nearly constant lattice parameter, as shown in Fig. 2, demonstrates a very low solubility of MgO in $Ce_{0.9}Gd_{0.1}O_{1.95}$, which agrees with the results reported by Cho et al. [9] and Inaba and Tagawa [22].

Fig. 3 shows FESEM micrographs of Mg-doped $Ce_{0.9}Gd_{0.1}O_{1.95}$ sintered at 1300 and 1500 °C. Some pores are observed in undoped $Ce_{0.9}Gd_{0.1}O_{1.95}$, and they disappear with increasing the content of MgO. It also can be found that MgO (dark phases) exists at the grain boundary, when Mg doping concentrations is ≥1 mol% confirmed by EDX (inset in Fig. 3(b)), which suggests 1 mol% is beyond the solubility limit. Therefore, the grain conductivity should scarcely be changed with adding more MgO, and the grain boundary conductivity may be affected, which is confirmed by the below discussions.

The average grain sizes of the specimens with various MgO concentrations are illustrated in Fig. 4. With the increase of the sintering temperature, the grain size of $Ce_{0.9}Gd_{0.1}O_{1.95}$ increases (from sub-micron to micron scale), and the grain size of MgO becomes larger simultaneously by Mg diffusion. Moreover, it can be seen from Fig. 4 that a large amount of MgO addition can suppress the grain growth, due to the segregation of MgO to the grain boundaries.

Different schematic equivalent circuits and corresponding ac impedance responses are shown in Fig. 5. Generally, in polycrystalline specimens, two independent semicircular arcs from high frequency to low frequency correspond to the conduction across the grains and grain boundaries, and a diffusion-limited process leads to an impedance response (Warburg impedance, Z_w) that appears as a straight line in the lower frequency range, as shown in Fig. 5(a). As the temperature is increased, the arcs are shifted into higher frequencies, which leads to the successive disappearance of grain and grain boundary arc (Fig. 5(b) and (c)). In the present case, in place of a capacitor, a constant phase element (CPE) was applied to fit the experimental data accounting for the microstructure inhomogeneity within the specimen.

At a given measuring temperature, an equivalent circuit was applied to fit the experimental data and then calculate the corresponding R_g and R_{gb}. In general, each individual resistance (shown in Fig. 5), R_i, can be formally converted to a conductivity σ_i, using the equation:

$$\sigma_i = \frac{l}{R_i S} \quad (1)$$

where l is the sample thickness and S is the electrode area of the sample surface. In this way, the total conductivity (σ_{tol}), the grain conductivity (σ_g), and the apparent grain boundary conductivity (σ_{gb}^{app}) can be obtained.

Fig. 6 shows the relationship of the total conductivity (σ_{tol}) of the samples with Mg concentrations at different sintering temperatures. It is shown that the total conductivity is affected by the doping content of Mg and sintering temperatures. When

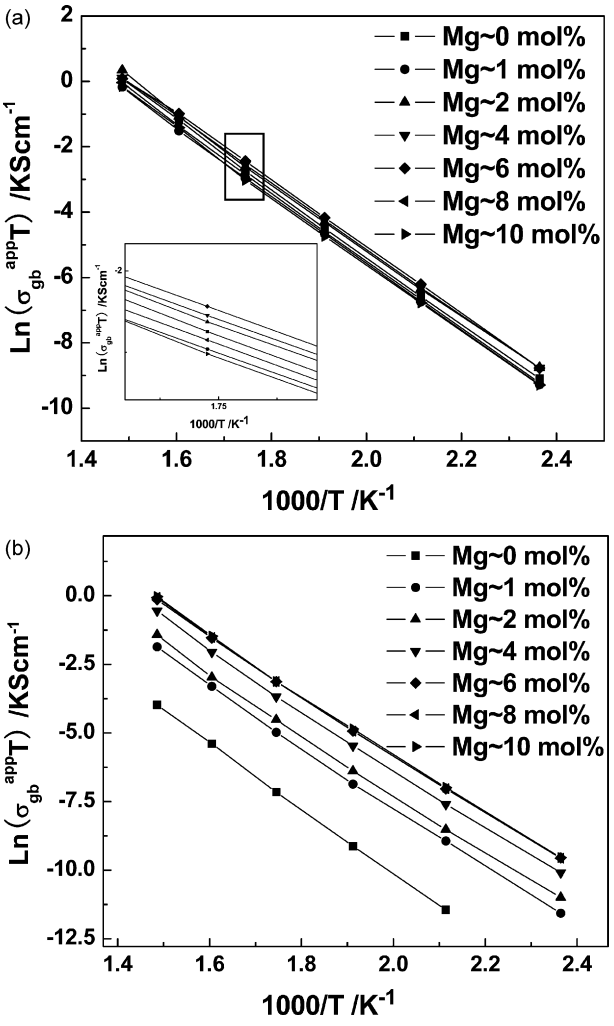

Fig. 8. The apparent grain boundary conductivity (σ_{gb}^{app}) of the samples with various Mg concentrations: (a) sintered at 1300 °C; (b) sintered at 1500 °C.

the sintering temperature is 1100 °C, σ_{tol} gradually decreases with increasing the doping content of Mg, and the undoped GDC exhibits the highest conductivity (such as, 1.02×10^{-2} S cm^{-1} at 600 °C in Fig. 6(a)). But as shown in Fig. 6(b), σ_{tol} of the samples sintered at 1300 °C increases (such as, from 1.34×10^{-2} up to 1.48×10^{-2} S cm^{-1} at 600 °C) with doping content of Mg up to 6 mol%, followed by a decrease, and the composition of 6 mol% turns up to be a turning point. However, σ_{tol} of the samples sintered at 1500 °C monotonously increases (such as, from 0.16×10^{-2} up to 1.31×10^{-2} S cm^{-1} at 600 °C, in Fig. 6(c)) as the doping content up to 10 mol%.

Fig. 7 shows the ac impedance spectra of the samples sintered at 1500 °C for 4 h with various Mg concentrations measured at 300 °C in air. As displayed in the inset of Fig. 7, it can be seen clearly that Mg doping content has negligible effect on the grain resistivity (ρ_g). This may be attributed to the very low solubility of Mg^{2+} in $Ce_{0.9}Gd_{0.1}O_{1.95}$ lattice. But the grain boundary conductivity varies with the MgO doping concentration, which is relative to the phenomenon that a majority of Mg^{2+} segregates into the grain boundary as shown in Fig. 3. As shown in Fig. 8, the trend of the apparent grain boundary conductivity with the doping content is consistent with that of the total conductivity, as a result of the constant grain resistivity.

The total activation energy (E_{tol}) and the grain boundary activation energy (E_{gb}) can be obtained via the plots of ln(σT) versus $1/T$ (as shown in Figs. 6 and 8), using the following equation:

$$\sigma T = \sigma_0 \exp\left(-\frac{E_i}{kT}\right) \quad (2)$$

where E_i represents E_{tol} or E_{gb}, and σ_0 is the pre-exponential factor being a constant in a certain temperature range, and k is Boltzmann constant. As reported by BCH Steele [23], a curvature point at about 400 °C existed in the Arrhenius curve of grain conduction for pure $Gd_{0.1}Ce_{0.9}O_{1.95}$, due to the different conduction mechanisms in different temperature ranges. In the present study, E_{tol} and E_{gb} are obtained in the lower temperature ranges of 150–400 °C. Fig. 9 shows E_{tol} and E_{gb} of the samples sintered at different temperatures as a function of MgO doping concentration. For the samples sintered at 1100 °C, E_{tol} is nearly constant. For the samples sintered at 1500 °C, E_{tol} sharply declines with increasing the doping content. And when the samples were sintered at 1300 °C, E_{tol} slightly decreases with increasing the Mg doping content, and reaches the minimum value of 0.84 eV at the Mg content of 6 mol%, and then

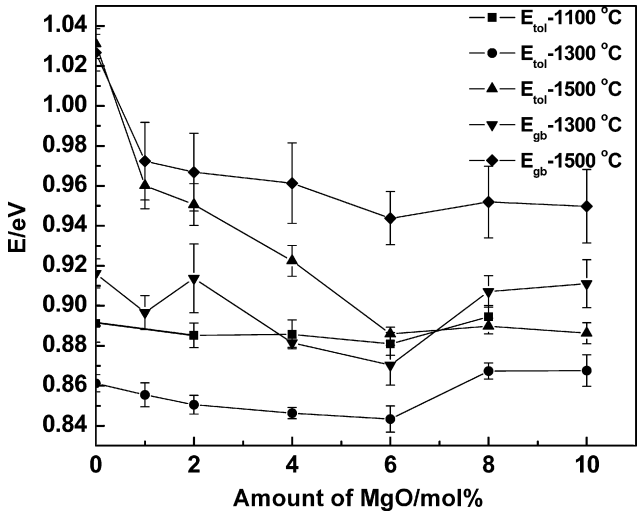

Fig. 9. The activation energy of total (E_{tol}) and grain boundary (E_{gb}) of the samples sintered at different temperatures as a function of MgO doping concentration.

increases. The presence of the turning point at 6 mol% coincides with the cases of the total and grain boundary conductivity. Similar trends about E_{gb} are observed in Fig. 9. As previously reported by Pérez-Coll et al. [6] and Sha et al. [7], E_{gb} is much larger than that of E_g, so E_{tol} is smaller than E_{gb} and E_{gb} is the dominating factor, which agree with our results.

It can be seen clearly from Fig. 8 that the addition of MgO can result in betterment on the grain boundary conductivity. The reasons may be, as follows: (1) the impurity of SiO_2 was scavenged; (2) the relative density of the conductive phases increased; (3) the improvement of the grain boundary conductivity resulting from space charge layer. As confirmed by Cho et al. [9], MgO can be used as SiO_2 scavengers to form $MgSiO_3$ perovskite at the grain boundary. In this study, according to the results of ICP, the SiO_2 wt.% was about 42 ppm (less than 50 ppm), and no compounds containing Si were formed by EDX (inset in Fig. 3(b)), so the reaction of MgO with SiO_2 may be neglected. Fig. 10 shows the relative density and the ratio of pure $Ce_{0.9}Gd_{0.1}O_{1.95}$ volume/the total volume (V_{GDC}/V_{tol}) of the samples sintered at different temperatures versus MgO doping concentration. V_{tol} is the sum of the volumes of

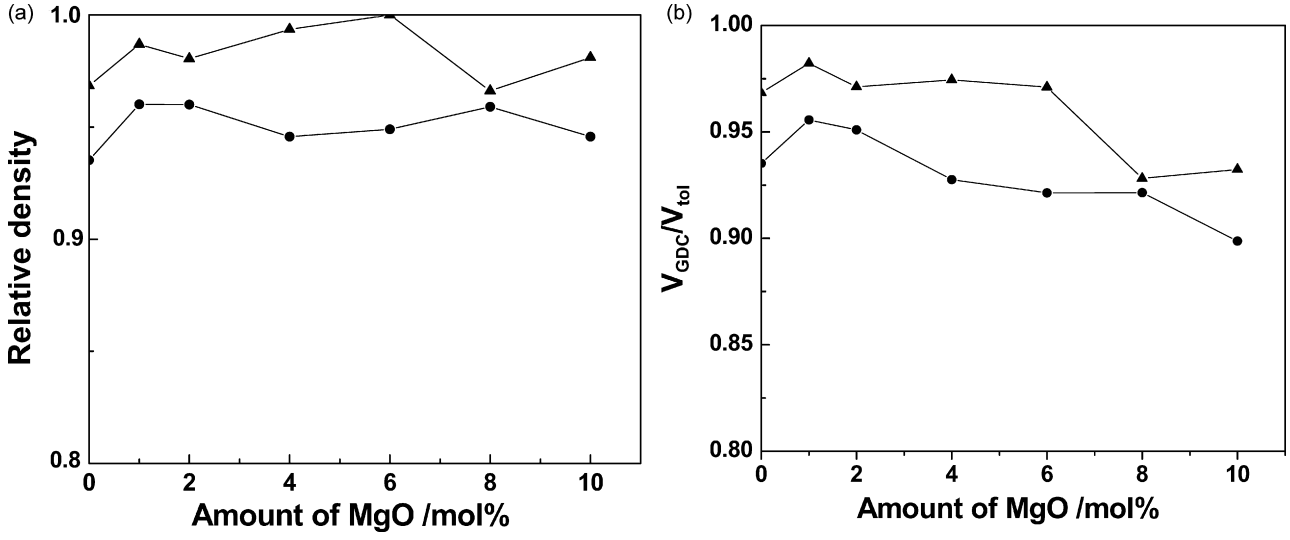

Fig. 10. The relative density and V_{GDC}/V_{tol} of the samples sintered at 1300 °C (●) and 1500 °C (▲) for 4 h vs. MgO doping concentration.

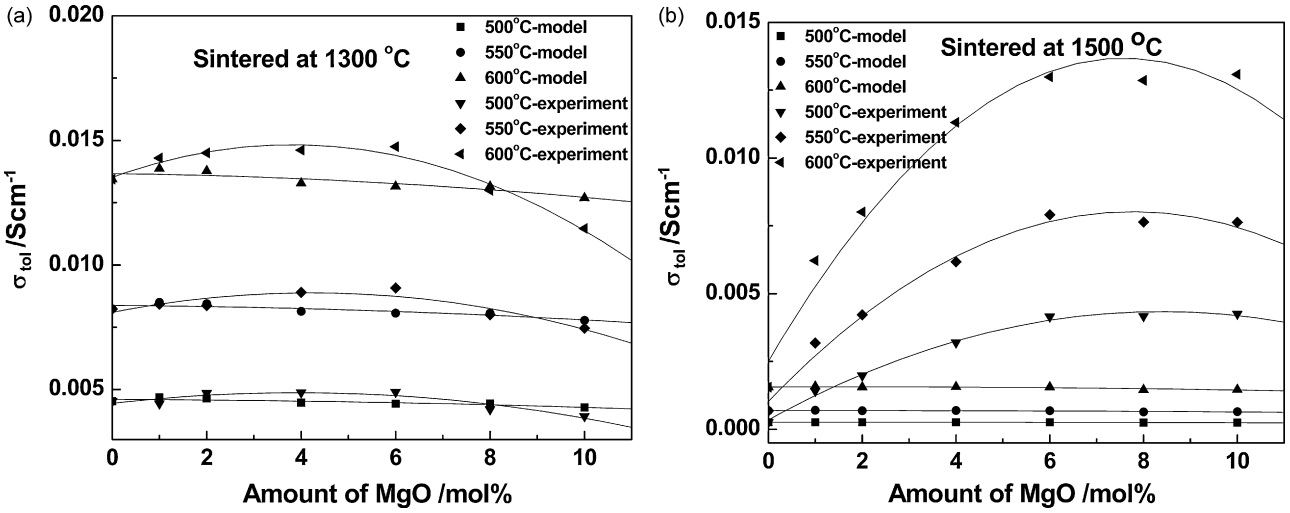

Fig. 11. The total conductivity (σ_{tol}) obtained according to the experiment and Hashin and Shtrikman's model measured at 500–600 °C in air. All the specimens were sintered at (a) 1300 °C and (b) 1500 °C for 4 h.

pure $Ce_{0.9}Gd_{0.1}O_{1.95}$ (without pores), pores and MgO. As is known, the pores and the MgO phases are all high-resistivity phases. Their conductivities were supposed to be zero. If we only consider the influence of V_{GDC}/V_{tol}, the upper conductivity bonds σ_u can be derived by Hashin and Shsrikman's work [24]:

$$\sigma_u = \frac{1 - f_{GDC}}{f_{GDC}/3\sigma_{GDC} - 1/\sigma_{GDC}} \quad (3)$$

where σ_{GDC} is the conductivity of pure $Ce_{0.9}Gd_{0.1}O_{1.95}$, and f_{GDC} is the volume fraction of pure $Ce_{0.9}Gd_{0.1}O_{1.95}$. Thus, Fig. 11 shows the total conductivity (σ_{tol}) obtained according to the experiment and Hashin and Shtrikman's model measured at 500–600 °C. Comparing with the upper limit of the values calculated by Hashin and Shtrikman's model, the enhancement of the experimental conductivity may be mainly originated from the variety of space charge layer regions, to the exclusion of the influence of the relative density of the conductive phases.

Browning et al. [25] and Ikuhara et al. [26] have confirmed the accumulation of acceptor cations in the grain boundaries for zirconia- and ceria-based materials by means of electron energy-loss spectroscopy (EELS) and energy-dispersive X-ray spectroscopy (EDXS). Based on their experiments, a space charge layer model was proposed by Guo and Waser [8]. That is, the accumulation of acceptor cations at the grain boundaries, as a result of elastic strain and Coulomb interactions, leads to the oxygen vacancy depletion in the vicinity of the grain boundary and subsequently the reduction of the grain boundary conductivity. In this study, the model can also be applicable. When MgO was added, two effects were shown. On the one hand, a very small amount of Mg^{2+} was perhaps dissolved in the grain boundary, suppressing the accumulation of Gd^{3+} due to Coulomb repulsion, which caused the increasing concentrations of oxygen vacancies near the boundary and thus the improvement of grain boundary conductivity. On the other hand, a majority of Mg^{2+} was gathered, and MgO, as a high-resistivity phase, was formed at the boundaries (Fig. 3), reducing the conductive grain to grain contact areas and thus decreasing the conductivity. Owing to the two antagonist influencing factors, the appropriate Mg doping content with the maximum conductivity value presented, as shown in Fig. 11(a).

It is known that the diffusion process of Gd^{3+} is relative to temperature. Although high sintering temperature can lead to the improvement of the density (Fig. 10(a)) and the reduction of high-resistivity grain boundary, simultaneously it might result in the well-developed space charge layer regions. Hence, the samples sintered at a proper sintering temperature, such as 1300 °C in this study, can have the highest conductivity. The phenomenon was also observed by other investigators [7,16,17], as mentioned in Section 1. However, the addition of MgO can largely weaken the influence of sintering conditions on the grain boundary conductivity. For example, as shown in Fig. 11(b), for the samples sintered at 1500 °C, the addition of MgO improves the grain boundary conductivity by over 10^2 times comparing with the undoped $Ce_{0.9}Gd_{0.1}O_{1.95}$, i.e., up to 2.72×10^{-2} S cm^{-1} at the composition of 10 mol% measured at 500 °C. This may be explained by the optimization of space charge layer.

4. Conclusions

In summary, Mg-doped $Ce_{0.9}Gd_{0.1}O_{1.95}$ with 0, 1, 2, 4, 6, 8 and 10 mol% MgO were successfully prepared by citric acid-nitrate low temperature combustion process. Very low solubility (less than 1 mol%) of Mg^{2+} in $Ce_{0.9}Gd_{0.1}O_{1.95}$ lattice was evidenced by XRD and FESEM results. The effects of Mg doping on the electrical properties under different sintering temperatures were investigated in detail. The grain conductivity hardly changed in all cases due to the low solubility. The samples sintered at 1300 °C exhibited the higher total conductivity than those sintered at 1100 and 1500 °C with the maximum value of 1.48×10^{-2} S cm^{-1} (measured at 600 °C) at the Mg doping content of 6 mol%, corresponding to the minimum total activation energy (E_{tol}) of 0.84 eV in lower temperature ranges of 150–400 °C. For the samples sintered at 1500 °C, the effect of Mg doping was particularly significant in that it produced an enhancement in the grain boundary conductance by over 10^2 times at the Mg doping content of 10 mol%, consistent with the remarkable reduction in E_{tol} and E_{gb}, as compared with undoped $Ce_{0.9}Gd_{0.1}O_{1.95}$. The addition of MgO largely weakened the influence of sintering conditions on the grain boundary conductivity.

Acknowledgment

This study was supported by the National Nature Science Foundation of China (Grant No. 50572042).

References

[1] V.V. Kharton, F.M.B. Marques, A. Atkinson, Solid State Ionics 174 (2004) 135–149.
[2] J.W. Fergus, J. Power Sources 162 (2006) 30–40.
[3] L. Anna, J. Skinner Stephen, J. Mater. Chem. 16 (31) (2006) 3161–3170.
[4] D.-J. Kim, J. Am. Ceram. Soc. 72 (1989) 1415–1421.
[5] L. Minervini, M.O. Zacate, R.W. Grimes, Solid State Ionics 116 (1999) 339–349.
[6] D. Pérez-Coll, P. Núñez, J.R. Frade, J.C.C. Abrantes, Electrochim. Acta 48 (2003) 1551–1557.
[7] X. Sha, Z. Lu, X. Huang, J. Miao, Z. Liu, X. Xin, Y. Zhang, W. Su, J. Alloys Compd. 433 (2007) 274–278.
[8] X. Guo, R. Waser, Prog. Mater. Sci. 51 (2006) 151–210.
[9] Y.H. Cho, P.-S. Cho, G. Auchterlonie, D.K. Kim, J.-H. Lee, D.-Y. Kim, H.-M. Park, J. Drennan, Acta Mater. 55 (2007) 4807–4815.
[10] D.K. Kim, P.-S. Cho, J.-H. Lee, D.-Y. Kim, H.-M. Park, G. Auchterlonie, J. Drennan, Electrochem. Solid State Lett. 10 (5) (2007) B91–B95.
[11] P.-S. Cho, S.B. Lee, D.-S. Kim, J.-H. Lee, D.-Y. Kim, H.-M. Park, Electrochem. Solid State Lett. 9 (9) (2006) A399–A402.
[12] T.S. Zhang, J. Ma, Y.J. Leng, S.H. Chan, P. Hing, J.A. Kilner, Solid State Ionics 168 (2004) 187–195.
[13] T.S. Zhang, J. Ma, S.H. Chan, J.A. Kilner, J. Electrochem. Soc. 151 (10) (2004) J84–J90.
[14] D. Pérez-Coll, P. Núñez, J.C.C. Abrantes, D.P. Fagg, V.V. Kharton, J.R. Frade, Solid State Ionics 176 (2005) 2799–2805.
[15] D. Pérez-Coll, D. Marrero-Lopez, P. Núñez, S. Piñol, J.R. Frade, Electrochim. Acta 51 (2006) 6463–6469.
[16] H. Li, C. Xia, M. Zhu, Z. Zhou, G. Meng, Acta Mater. 54 (2006) 721–727.
[17] D.R. Qu, T. Mori, F. Ye, M. Takahashi, J. Zou, J. Drennan, Acta Mater. 54 (2006) 3737–3746.
[18] V.V. Kharton, F.M. Figueiredo, L. Navarro, E.N. Naumovich, A.V. Kovalevsky, A.A. Yaremchenko, A.P. Viskup, A. Carneiro, F.M.B. Marques, J.R. Frade, J. Mater. Sci. 36 (2001) 1105–1117.
[19] H. Xu, H. Yan, Z. Chen, J. Power Sources 163 (2006) 409–414.
[20] M.I. Mendelson, J. Am. Ceram. Soc. 52 (1969) 443–446.
[21] R.D. Shannon, C.T. Prewitt, Acta Crystallogr. B25 (1969) 925.
[22] H. Inaba, H. Tagawa, Solid State Ionics 83 (1996) 1–16.
[23] B.C.H. Steele, Solid State Ionics 129 (2000) 95–110.
[24] Z. Fan, Acta Metall. Mater. 43 (1995) 43–49.
[25] Y. Lei, Y. Ito, N.D. Browning, T.J. Mazanee, J. Am. Ceram. Soc. 85 (2002) 2359–2363.
[26] Y. Ikuhara, P. Thavorniti, T. Sakuma, Acta Mater. 45 (1997) 5275–5284.